

IN SITU, DOPPLER RADAR, AND VIDEO OBSERVATIONS OF THE INTERIOR STRUCTURE OF A TORNADO AND THE WIND–DAMAGE RELATIONSHIP

BY JOSHUA WURMAN, KAREN KOSIBA, AND PAUL ROBINSON

Observations inside a tornado, integrated with fine-resolution rapid-scan Doppler on Wheels data, and real-time observations of damage, reveal for the first time the three-dimensional structure of a tornado near the ground and help evaluate the enhanced Fujita scale.

THERE ARE FEW NEAR-GROUND OBSERVATIONS INSIDE TORNADOES.

Tornadoes cause substantial loss of life and property every year, primarily in the central regions of North America. In 2011, several hundred people lost their lives and over 20 billion dollars (all values are in current U.S. dollars) of damage occurred as the result of several tornado outbreaks that impacted populated regions (Lott et al. 2012; FEMA 2012). Verification of near-surface tornado wind models (Lewellen 1976; Church et al. 1979; Rotunno 1979; Davies-Jones 1986;

Lewellen et al. 1997; Lewellen et al. 2000; Lewellen and Lewellen 2007a,b; Snow 1982; Fiedler and Rotunno 1986) and the relationship between these winds and structural damage requires reliable measurements near the ground, in the core flow region of tornadoes. In recent years, mobile Doppler radars have been central to mapping the three-dimensional wind structure in many tornadoes from as low as 30 m above ground level (AGL) to above 1 km AGL. These have allowed the documentation of the evolution and structure of tornadic winds including the prevalence of axial down-drafts aloft, low-level convergence, and the existence of multiple vortices (Wurman et al. 1996; Wurman and Gill 2000; Bluestein et al. 2003, 2004; Wurman and Alexander 2005; Wurman and Samaras 2004; Bluestein et al. 2007; Wurman et al. 2007a,b,c; Wurman 2002; Kosiba et al. 2008; Lee and Wurman 2005; Tanamachi et al. 2007; Wurman and Kosiba 2008; Wurman et al. 2008; Kosiba and Wurman 2010; Wurman et al. 2010; Wurman and Kosiba 2013, manuscript submitted to *Wea. Forecasting*). However, the structure of tornadic winds below ~30 m AGL has not been well quantified. Radar measurements, with few exceptions (Wurman

AFFILIATIONS: WURMAN, KOSIBA, AND ROBINSON—Center for Severe Weather Research, Boulder, Colorado

CORRESPONDING AUTHOR: Joshua Wurman, Center for Severe Weather Research, 1945 Vassar Circle, Boulder, CO 80305
E-mail: jwurman@cswr.org

The abstract for this article can be found in this issue, following the table of contents.

DOI:10.1175/BAMS-D-12-00114.1

In final form 19 October 2012
©2013 American Meteorological Society

and Alexander 2005; Wurman et al. 2007a; Kosiba et al. 2008; Kosiba and Wurman 2012), seldom extend much below 30 m AGL because of radar beam spreading and intervening terrain, flora, and manmade structures. The rare radar measurements that do exist in the 4–30-m AGL region reveal little reduction in wind speeds between 100 and 200 m AGL and the lowest observed levels (Wurman et al. 2007a).

Measurements of tornadic winds are challenging to obtain since tornadoes are small, difficult to predict, short-lived, and do not propagate along easily forecast tracks. Additionally, obtaining in situ measurements is extremely difficult since the interior environment of tornadoes is characterized by intense winds and rapidly moving airborne debris hazardous to instrumentation and observers. Infrequent near-surface (1–3 m AGL) wind data obtained at the edges of tornadoes suggest only a modest drop in ground-relative V_g and tornado-relative V wind speeds below the lowest frequently radar-observed levels (~100 m AGL) (Wurman et al. 2007a). These occasional 1–3-m AGL observations have been inconclusive regarding the intensity of radial wind speeds, V_r , with some observations suggesting nearly pure tangential flow V_t with little or no spiraling inflow ($V_r \ll V_t$) and others suggesting intense inflow with $V_r > V_t$. This may be due to variations among tornadoes, azimuthal variations, or even localized and/or transient inflow jets in individual tornadoes. Since the in situ measurements alone result in only one-dimensional slices immediately near the ground, inferring three-dimensional vortex structure is problematic. While these data have revealed tantalizing information concerning the interior and immediate surroundings of tornadoes, they have not previously allowed the reconstruction of the near-surface three-dimensional winds.

LITTLE FIELD DATA SUPPORTING WIND–DAMAGE RELATIONSHIPS. In addition, the relationship between tornadic winds and damage is poorly understood. Recently the operational model used to infer peak tornado wind speeds from observed damage has been substantially modified and renamed the enhanced Fujita (EF) scale, modifying the wind gust speeds assumed to cause different intensities of damage (Wind Science and Engineering Center 2006; McDonald et al. 2004; Potter 2007; Doswell et al. 2009; Edwards et al. 2013). While this

wind–damage relationship is used officially by the National Weather Service to estimate wind speeds, the new wind–damage relationships are based on “expert elicitations” and post-tornado damage surveys rather than empirical evidence relating specific damage events occurring during a tornado to measured winds in different locations within a tornado. Up until now, there has existed no direct intercomparison between anemometer-measured winds and real-time documentation of damage within a tornado. Model simulations (Fouts et al. 2003; Selvam and Millett 2003; Kuai et al. 2008; Haan et al. 2010) and occasional comparisons of radar-measured winds to damage (Wurman and Alexander 2005) have questioned some of the unverified assumptions of these damage–wind speed relationships, including the underlying assumption that damage is caused by the peak 3-s duration winds at 10 m AGL, without accounting for changes in the wind direction, speed, cumulative effects of longer duration intense winds, or the effects of impacts from airborne debris (e.g., breaking windows and/or doors, permitting wind to enter structures, resulting in upward wind loading on roofs). Accurate verification and quantification of the relationship between tornadic winds and damage requires direct comparisons between observed damage and measured winds in actual tornadoes.

INTEGRATED WIND, VIDEO, AND RADAR INSIDE TORNADO REVEAL 3D STRUCTURE. Just after 2152 UTC (hereinafter all times are UTC) on 5 June 2009, a tornado formed in Goshen County, Wyoming. It was observed by multiple instruments deployed for the second phase of the Verification of the Origins of Rotation in Tornadoes Experiment (VORTEX2) (Wurman et al. 2012; Kosiba et al. 2013; Markowski et al. 2012a,b; Wakimoto et al. 2011, 2012; Atkins et al. 2012), for its entire life-cycle until it dissipated at 2230 (Fig. 1). The tornado was given an EF-2 rating by the National Weather Service based partially on preliminary Doppler on Wheels (DOW) (Wurman et al. 1997; Wurman 2001; Wurman et al. 2008) observations. Peak winds in the tornado were measured at about 2214, at which time Rapid-Scan DOW (RSDOW) measurements revealed Doppler velocities V_d of 72 m s^{-1} at 30 m AGL.¹ The DOWs (Fig. 2, bottom) are a network of mobile Doppler radars that have pioneered the finescale

¹ This measurement is near the EF-3/EF-4 threshold. Even though the observations were at 30 m AGL, it is likely, based on evidence in other tornadoes (Wurman et al. 2007a) and the evidence presented here, that the intensity of radar-observed winds at 30 m AGL is close, within 10%–20%, to that of standard-height 10-m AGL winds. This RSDOW measurement was not available to the National Weather Service at the time they made their EF-2 damage intensity rating.

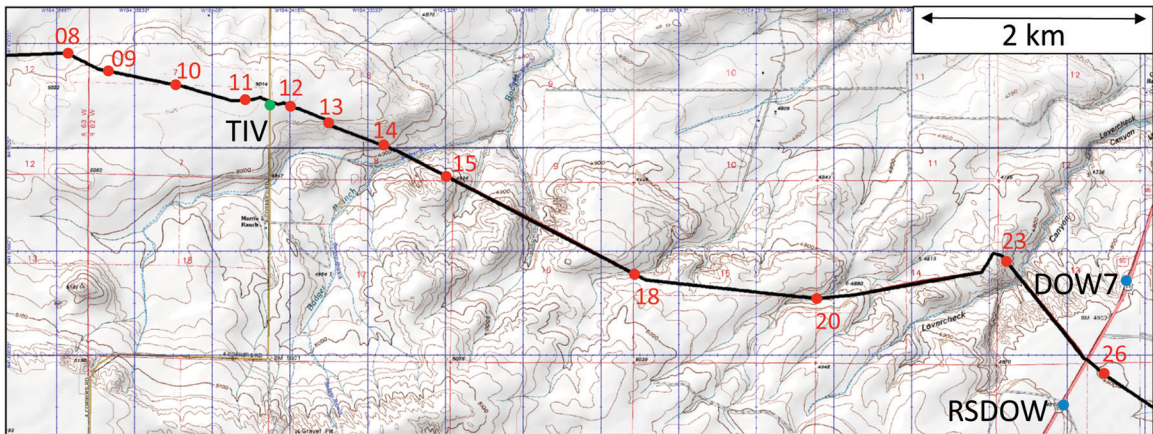


FIG. 1. Rapid-scan Doppler on Wheels (RSDOW), Doppler on Wheels 7 (DOW7) (blue dots), and Tornado Intercept Vehicle (TIV) (green dot), and track of the center of rotation of the tornado (black line). Labels adjacent to red dots are time in minutes after 2200 (all times are UTC). Also shown are terrain contours (brown, in feet). Four Corners Road (brown line), and Highway 85 (red line). The tornado center passes from west to east, 35 m north of the TIV at closest approach, at 2211:29.

observations of tornado structure and other small-scale and rapidly evolving phenomena (e.g., Wurman et al. 1996; Marquis et al. 2007; Wurman and Winslow 1998). Briefly, the DOWs operate at a wavelength near 3.2 cm, transmit narrow, $\sim 0.9^\circ$ wide beams, and scan quickly both vertically and horizontally to collect volumetric data. The Rapid-Scan DOW (RSDOW) (Wurman et al. 2008) transmits six simultaneous vertically stacked beams to provide rapid, 7-s, volumetric updates. Returned signals in all DOWs are processed to provide Doppler velocity, radar reflectivity, and other quantities. A detailed description of the DOW data collection, scanning strategy, deployments, and data processing used during this storm is discussed by Kosiba et al. (2013). In addition to the VORTEX2 instrumentation, the instrumented and armored Tornado Intercept Vehicle (TIV) (Wurman et al. 2007a) (Fig. 2, top) targeted the tornado. The TIV is a truck, modified and armored to facilitate the IMAX-format documentary filming inside tornadoes and supports a mast with an RM Young 5103 anemometer at 3.5 m AGL as well as other meteorological instrumentation. TIV wind and other meteorological data were recorded on a Campbell Scientific CR1000 data logger at 1-s intervals while video was collected from several vehicle-mounted and handheld cameras, as well as an IMAX-format film camera. Combined TIV and DOW observations provided the unique opportunity to integrate radar and in situ wind and video data to address outstanding questions related to the low-level tornadic wind structure and wind–damage relationships.

RSDOW data revealed the tornado crossed Four Corners Road at 41.62872°N , 104.34386°W at 2211:29.



FIG. 2. (top) The TIV. (bottom) A DOW.

At that time, the tornado had a radar-determined radius (R_r ; defined by $\frac{1}{2}$ the distance between the peak outbound and inbound V_d measurements) of about 105 m, a debris ring with radius near 200 m,

and a propagation velocity V_p of 7.5 m s^{-1} toward 110° (east southeastward) (Fig. 3).² (An animation of the RSDOW radar imagery during this period is available online at www.cswr.org/BAMS-goshen.html). Less than a minute earlier, at 2210:46, the TIV deployed on Four Corners Road, at 41.62840°N , 104.34386°W , in the path of the tornado.³ The terrain along the tornado track well west and at least 1 km east of the TIV, including the study period, was relatively flat and quite open although it became hilly to the east (Fig. 1). Video imagery taken from the TIV reveals a landscape dominated by grass. “Low grass, steppe” is associated with short roughness lengths of approximately 0.01–0.04 m (Simiu and Scanlan 1996). At 2211:31 the center of the tornado circulation passed 35 m north-northeast of the TIV (Fig. 4). As the tornado approached the TIV, anemometer-measured ground-relative winds V_g increased to 51 m s^{-1} at 2211:18 (when averaged over 3 s, $V_g = 47 \text{ m s}^{-1}$) (Fig. 5), decreased to 31 m s^{-1} inside of the tornado by 2211:31, and then increased to 58 m s^{-1} by 2211:40–2211:43 (3-s average = 56 m s^{-1} at 2211:43).⁴ By 2212, wind speeds had decreased to 42 m s^{-1} , as the center of the tornado moved away.⁵ Wind direction veered from south to northwesterly during the passage of the tornado. Atmospheric pressure dropped about 2,000 Pa (20 mb)

to a minimum at 2211:25. TIV-measured wind speed and pressure reached relative minimums within few seconds of the independently DOW-measured time of closest approach of the center of tornado circulation, providing confidence in the spatial and temporal accuracy and navigation of the DOW and TIV data.

TIV observations during the passage of the tornado resulted in a transect of V_g through a chord of the tornado, passing as close as 35 m from the center of circulation (Fig. 4). This permitted the calculation of the principal horizontal components of the tornado wind field, V_r and V_t from $35 < R < 120 \text{ m}$, where R is the distance from the center of rotation, using the DOW-measured $V_p = 7.5 \text{ m s}^{-1}$ toward 110° . Profiles of V (total tornado-relative velocity), V_p and V_r were created during both the approach and retreat of the center of the tornado (Fig. 6). The radius of maximum V , RMV, was 100 m, similar to the DOW-measured R_t above the TIV, with $V = 50 \text{ m s}^{-1}$. The radius of maximum V_p , RMVT, was 65 m, meaning that peak V_g was outside the circle of peak V_r . Asymmetry was evident, with maximum $V_t = 40 \text{ m s}^{-1}$ in the southeast sector and $V_t = 30 \text{ m s}^{-1}$ in the southwest sector. In the southwest sector, strong inward $V_r = -40 \text{ m s}^{-1}$ at $R = 100 \text{ m}$ decreased roughly linearly to -15 m s^{-1} at $R = 35 \text{ m}$, consistent with a Burgers–Rott wind profile (Burgers 1948; Rott 1958),⁶ resulting in

² Doppler velocity errors are difficult to quantify and can be caused by many factors, including reflectivity weighting resulting in misrepresentative “mean” Doppler velocities, nonterminal velocity scatterers such as debris (Dowell et al. 2005), sidelobe contamination, and underlying noise in the measurements. Discussion of these is beyond the scope of this paper. Based on spatial and temporal continuity, it is likely that individual Doppler values are accurate within 5% or $\pm 2\text{--}3 \text{ m s}^{-1}$.

³ The DOWs were deployed at lower elevations than the TIV. The DOW7 antenna was at 1,488 m MSL (above mean sea level) and the Rapid-Scan DOW antenna was at 1,501 m MSL, while the ground elevation at the TIV was 1,531 m MSL. Therefore, the center of the lowest radar beams crossed over the TIV at approximately 20 m AGL. However, velocities in these lowest beams were often contaminated by ground clutter returns and data from 90 to 100 m AGL were used in some calculations.

⁴ The anemometer manufacturer states that wind speed accuracy is 1% and directional accuracy is 3° (www.youngusa.com/Brochures/05103%280106%29.pdf).

⁵ There is no accepted definition for the outer boundary of a tornado, so it is difficult to specify when the TIV and its anemometer were “inside” versus “outside” the tornado. Visual observers frequently define the outer boundary of a tornado as either the edge of the debris cloud or condensation funnel, but these definitions are problematic since they depend on ground conditions, atmospheric visibility, proximity to the tornado, lighting, and the humidity of the air flowing into the tornado, not just the kinematic structure. DOW measurements, when collected from close enough ranges to resolve the tornadic flow, result in a well-defined and kinematically based metric, defining the inside of a tornado as the region enclosing the maximum difference in velocity. But these measurements are only available rarely, perhaps in 1% of tornadoes. Damaging winds, lofted debris, and condensation can occur well outside the region enclosed by maximum velocity. Conversely, in rapidly propagating and/or weaker tornadoes, little or no damage may occur on the weak (left relative to V_p) side of the path of the center of the tornado where V_t generally opposes V_p , resulting in less intense V_g .

⁶ The Burgers–Rott model provides a solution to the axisymmetric angular momentum equation by assuming the inward radial advection of angular momentum is balanced by the outward radial diffusion of angular momentum by viscosity, $V_t = G[1 - \exp(-aR^2/2n)]/(2pR)$, $V_r = -aR$ for $R < 65 \text{ m}$, $a = 0.45 \text{ s}^{-1}$, $G = 38,000 \text{ m}^2 \text{ s}^{-1}$, and $n = 1,800 \text{ m}^2 \text{ s}^{-1}$, where a is a constant, G is circulation, and n is viscosity. To reproduce decreasing winds outside RMV, $V_r = -0.64V_t$ for $R > 65 \text{ m}$ (constant pitch spiraling wind). This profile approximately matched observed V_g and V , V_p and V_r at the TIV (Fig. 6), although there are deviations due to both asymmetries in the tornado structure and the dynamical difference in the flow regime at 3.5 m AGL compared to that assumed in the model. No claim is made that the balance assumed in the Burgers–Rott model is suggested by the 3.5-m anemometer data.

the observed $RMV > RMVT$. The comparison with a Burgers–Rott profile is intended to be approximate. The aforementioned asymmetries are not represented in the modeled profiles and the available data did not permit a detailed analysis of these asymmetries. The measured pressure deficit was somewhat less than predictions based on cyclostrophic balance using the observed V_r profiles, probably due to unbalanced and transient flow near the ground.

RSDOW observations every 7 s revealed a periodicity in tornado intensity, with amplitude of $\sim 4 \text{ m s}^{-1}$ and peak energy at periods of 66 and 108 s (Fig. 7). This is consistent with long wavelength, upstream-propagating Rossby-type waves slowly revolving about the tornado at $6\text{--}10 \text{ m s}^{-1}$, not short wavelength multiple-vortex type phenomena that would complete orbits in $\sim 20 \text{ s}$ (e.g., Wurman 2002; Nolan and Montgomery 2002; Wurman and Kosiba 2013, manuscript submitted to *Wea. Forecasting*). No multiple vortices were observed visually (Wakimoto et al. 2011; Atkins et al. 2012), and while peak V_g was higher in the southwest sector of the tornado (2211:43 in Fig. 5), values of V were very similar at comparable R in both sectors (Fig. 6). While variations in surface roughness, lofted debris, and other conditions could cause modulation in low-level wind intensity (e.g., Lewellen et al. 2008), the observed oscillatory behavior is present from 2210 to 2213, during which the tornado is crossing relatively flat and homogeneously grassy terrain (Fig. 1).

Models of tornado flow (Lewellen 1976; Davies-Jones 1986; Lewellen et al. 1997; Lewellen et al. 2000; Lewellen and Lewellen 2007a,b; Snow 1982; Fiedler and Rotunno 1986) predict that within the RMV tornadoes may contain updrafts, downdrafts, or both. Radar

observations suggest updrafts or downdrafts may be present (Wurman et al. 1996; Wurman and Gill 2000; Bluestein et al. 2003; Wurman 2002; Kosiba et al. 2008; Lee and Wurman 2005; Tanamachi et al.

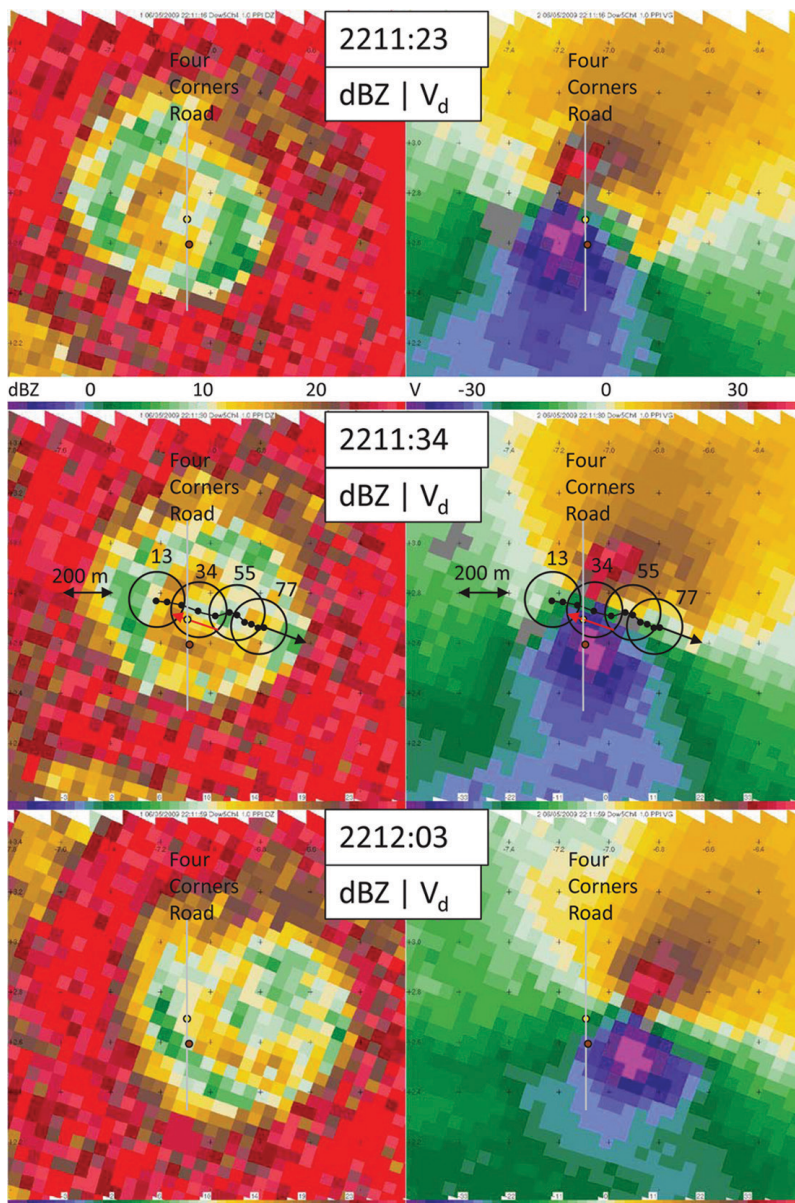


FIG. 3. (left) Radar reflectivity (dBZ) and (right) Doppler velocity (V_d) in the Goshen County, Wyoming, tornado at (top) 2211:23, (middle) 2211:34, and (bottom) 2212:03 5 Jun 2009 as observed by the Rapid-Scan DOW radar as the tornado crosses over the TIV (yellow dot) and pole 100S (red dot). The center of rotation of the tornado, surrounded by an approximately 105-m region between maxima in V_d (black dots and circles, labeled with seconds after 2211:00), crosses 35 m north-northeast of the TIV at 2211:31, resulting in a transect of the core flow region (red arrow) from 2211:18 to 2211:43. A moderate-intensity (yellow and brown) reflectivity debris ring surrounding tornado is clearly visible, as is higher reflectivity (red) associated with rain and hail observed at the TIV before and after the tornado's passage. Black tick marks are spaced at 200-m intervals.

2007; Kosiba and Wurman 2010) and that downdrafts penetrating as low as the lowest radar-observed level may predominate (Alexander and Wurman 2008). To evaluate the updraft/downdraft structure in this tornado near the surface, the vertical component of wind velocity W at 7 m AGL (twice the TIV anemometer height) was derived from the vertical momentum

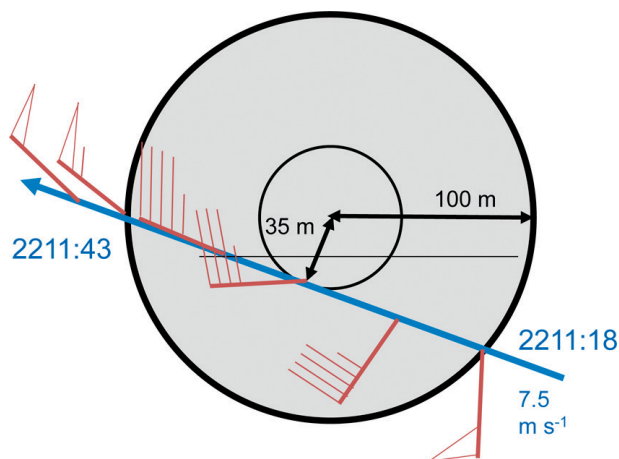


FIG. 4. Schematic illustration of transect of tornado by the TIV. The tornado, with a radius of maximum winds of 100 m, propagates toward 110° at 7.5 m s^{-1} , with the center of circulation passing 35 m north-northeast of the TIV, resulting in measurements through a chord of the tornado as shown. Wind barbs show measurements of V_g at 3.5 m AGL with pennants indicating 50 m s^{-1} , full barbs 10 m s^{-1} , and half barbs 5 m s^{-1} .

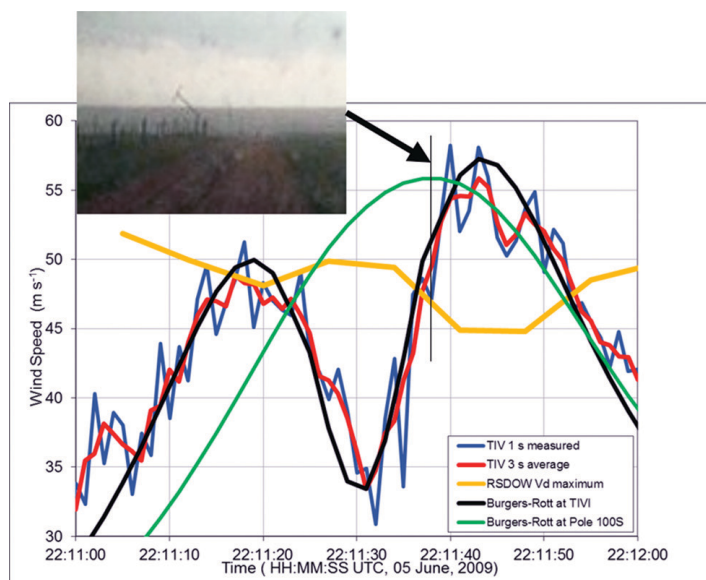


FIG. 5. TIV-measured wind speeds inside tornado every 1 s (blue), averaged for 3 s (red). Modeled winds at the TIV (black) and at pole 100S (green). Peak RSDOW V_d (yellow). Zoomed in video image of pole 100S snapping at 2211:38.

equation using V_r and V_t and assuming mass conservation, incompressibility, and $W(0 \text{ m AGL}) = 0 \text{ m s}^{-1}$. Upward motion of $\sim 7 \text{ m s}^{-1}$ was calculated from $35 < R < 120 \text{ m}$, although there was considerable spread, between -1 and $+14 \text{ m s}^{-1}$ for $R < 55 \text{ m}$ (Fig. 6). This observation of $W \ll V$ is consistent with video evidence that revealed predominantly horizontal motion of small debris, primarily grass, within a few meters AGL.

RSDOW data were interpolated to a Cartesian grid [using a Barnes (1964) scheme with $\kappa = 0.0016 \text{ km}^2$ and grid spacing = 20 m] in order to derive the axisymmetric three-dimensional winds (V_r , V_t , and W) aloft in and near the tornado using the ground-based velocity track display (GBVTD) method, which was originally developed to analyze hurricane vortices (Lee et al. 1999) and has since been extended to resolve tornadic structure (Bluestein et al. 2003; Lee and Wurman 2005; Bluestein et al. 2007; Tanamachi et al. 2007; Kosiba and Wurman 2010). This revealed maximum V_t near 40 m s^{-1} with RMVT = 150 m, greater than RMVT calculated from anemometer data (Fig. 8). This difference was likely due either to the widening and weakening of the tornado between the ground and the lowest radar-observation level used in the GBVTD analysis, and/or to spatial smoothing in the GBVTD analysis. Aloft, the GBVTD-derived winds revealed an axial downdraft with peak W of $\sim 10 \text{ m s}^{-1}$ and weak outflow/divergence inside the RMVT, which was in contrast to the strong inflow measured near the ground. Recall that in situ video evidence obtained by the TIV, below the lowest GBVTD level, indicated predominantly horizontal inward-spiraling near-surface winds, and analysis of anemometer data revealed modest upward motion at 7 m AGL.⁷

The temporal variability of the profiles of V_t and V_r is about 5 m s^{-1} . These may be manifestations of asymmetries in tornado structure, which may be better or more poorly resolved by the radar at different times, actual tornado evolution, or errors

⁷ The Barnes analysis was extrapolated below the lowest radar observation level, and a boundary condition of $W = 0$ at the ground was imposed. With no evidence that the 3.5-m AGL TIV observations were representative well above the surface, and the likelihood that the observed inflow was shallow, these observations were not interpolated upward. Different boundary conditions could affect the GBVTD-retrieved W .

in the GBVTD analysis. The overall consistency of the retrieved bulk structure provides confidence in the validity of the analysis.

During the transect, peak V_d at 20–90 m AGL ranged from 45 to 52 m s^{-1} (Fig. 5), less intense than TIV-measured peak V_g , suggesting that the most intense V_g was likely between 3.5 and 20 m AGL. However, due to spatial smoothing in the radar data, these observations are also consistent with nearly constant V_g from 3.5 to 90 m AGL, as found previously (Wurman et al. 2007a). Critically, for the overwhelming majority of analyses of tornadoes, which employ radar data only from >30 m AGL and lack contemporaneous in situ data, wind speeds at ~10 m AGL are not substantially less than those measured at the lowest radar-observed levels.

A three-dimensional model of this tornado's structure was created using the combined anemometer, video, and DOW data from this study (Fig. 9). Strong inward-spiraling near-surface inflow approached the tornado center and then rose at a moderate, approximately constant speed. Aloft, an axial downdraft penetrated to below 100 m AGL, and inflow was much weaker and did not approach the center of circulation. This reconstruction is consistent with the range of structures predicted in tornadoes (Lewellen 1976; Davies-Jones 1986; Howells et al. 1988; Church and Snow 1993; Lewellen et al. 1997) and observed by radar (Wurman et al. 1996; Wurman and Gill 2000; Wurman and Alexander 2005; Bluestein et al. 2007; Wurman et al. 2007a; Tanamachi et al. 2007; Kosiba et al. 2008; Kosiba and Wurman 2010), although the axial downdraft intensity is substantially smaller than previously observed (Wurman et al. 1996; Wurman and Gill 2000; Kosiba et al. 2008; Kosiba

Approaching solid circles, Departing open circles

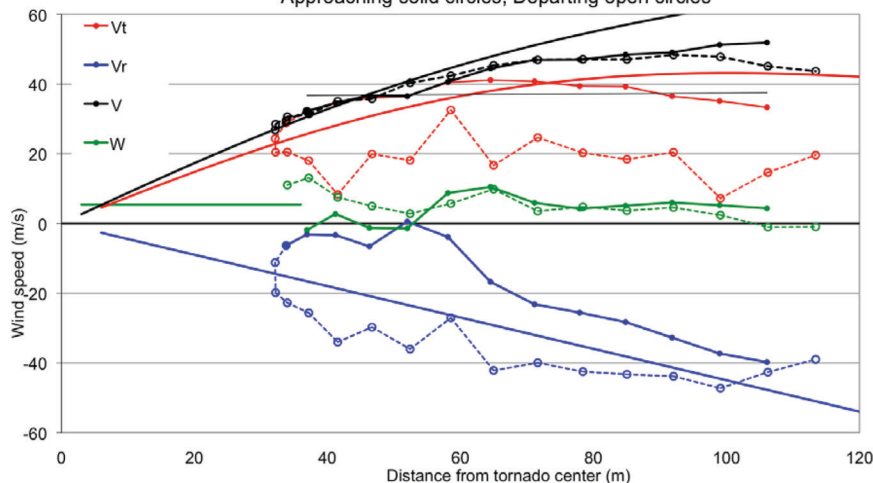


FIG. 6. Profiles from data (marked lines) and Burgers–Rott modeled (unmarked lines) V_t , V_r , V , and W versus R . Data collected during tornado approach (departure) are indicated with solid (open) circles. Strong inward and upward motion is present from $35 < R < 120$ m.

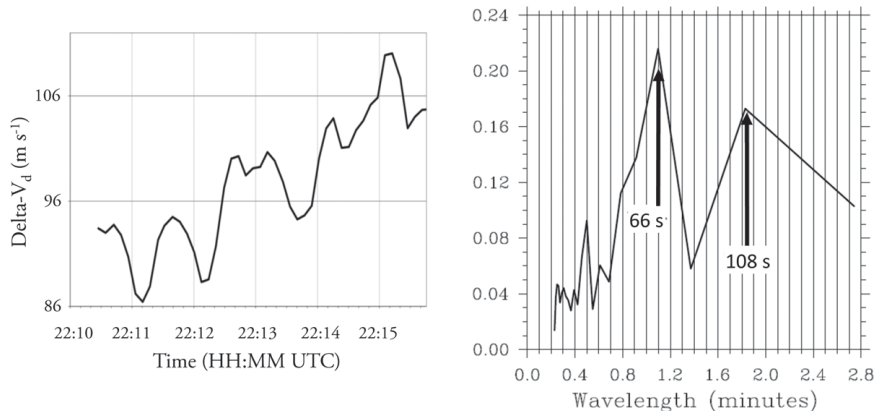


FIG. 7. (left) Oscillation of tornado intensity defined by maximum $\Delta V = V_d(\text{outbound}) - V_d(\text{inbound})$. (right) FFT of ΔV with peak energy at 66 and 108 s, suggestive of rotating asymmetry in vortex.

and Wurman 2010). Significantly, this “divided” vertical structure suggests that the largest winds occur between the surface and the height of the downdraft (Fiedler and Rotunno 1986; Church and Snow 1993) and therefore it is likely that the maximum wind speed occurred between the radar-observed and anemometer-observed levels. Potentially interesting structural features in the corner flow region between 3.5 and 30 m AGL were not resolved in this study and are not represented in the deduced three-dimensional model.

COMPARISONS OF WINDS AND DAMAGE. The time history of V_g at all near-ground points impacted by the tornado was calculated by fitting a modified Burgers–Rott vortex

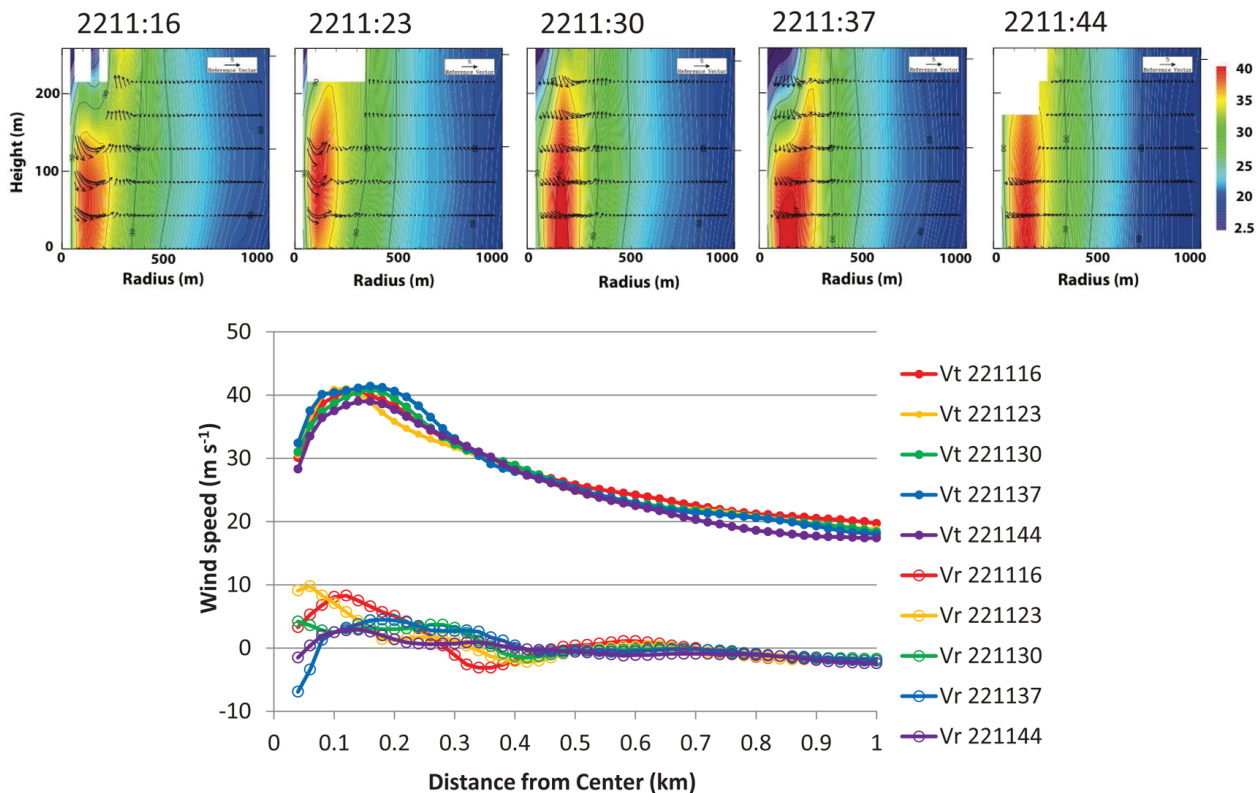


FIG. 8. Axisymmetric radial and tangential wind profiles derived from the RSDOW using the GBVTD technique, using the lowest clutter-free scan near 100 m AGL. (top) Vertical cross sections illustrating maximum V_t at $R = 100\text{--}200$ m and $W < 0$ from $0 < R < 200$ m. GBVTD cross sections extend from $0 < R < 1,000$ m horizontally and $0 < z < 250$ m AGL vertically. Reference vector is 5 m s^{-1} . (bottom) Azimuthally averaged V_t and V_r as a function of radius. Generally outward (divergent) flow is present from $0 < R < 250$ m.

wind profile (Burgers 1948; Rott 1958) of V_r and V_t to the TIV transect data (Fig. 5). This allowed for the temporal evaluation of V_g as the tornado damaged a line of wire-connected wooden electrical transmission poles, including one adjacent to the TIV (pole A), one 100 m to the south (pole 100S) (Figs. 3 and 5), and a pole 200 m south of the TIV (pole 200S) (not shown). The value of V_g at pole 100S increased to a maximum of 56 m s^{-1} at 2211:38 as the wind direction veered from south to west northwesterly. Video revealed that pole 100S snapped at 2211:38, near the time of maximum V_g at pole 100S, dragging down the poles farther to the south (e.g. Pole 200S). Pole A also snapped at 2211:38, nearly simultaneously with pole 100S, when measured-TIV winds were $V_g = 49\text{ m s}^{-1}$ from the west-northwest, but that location experienced more intense winds after pole A snapped. Pole A may have been very near failure and dragged down by the added stress caused by the falling wires connected to pole 100S or it may have failed independently. Pole A had survived TIV-measured winds of 51 m s^{-1} from the southwest several seconds earlier, at 2211:18. (An excerpt from

the video of the poles snapping is available online at www.cswr.org/BAMS-goshen.html.)

The EF scale (Wind Science and Engineering Center 2006; McDonald et al. 2004; Potter 2007; Edwards et al. 2013) suggests that wooden electrical transmission line poles should fail at an “expected” wind speed of 53 m s^{-1} , with the lower bound of all expert elicitations being 44 m s^{-1} . Pole 200S experienced peak wind gusts of only 39 m s^{-1} at the time it failed, substantially lower than these EF-implied destruction thresholds (and only slightly above the “threshold of visible damage” at 37 m s^{-1}). Pole 200S is seen in the video to have been dragged down by wires connecting it to pole 100S and not destroyed directly by the local peak wind gusts themselves. Pole A snapped at a wind speed, $V_g = 49\text{ m s}^{-1}$, below the EF-scale expected prediction, but winds exceeded the expected threshold after damage was complete. Pole 100S survived the EF-scale expected wind speed of 53 m s^{-1} , then failed at 56 m s^{-1} , which is below the “upper bound” wind speed of 63 m s^{-1} . The EF-scale descriptive document (Wind Science and Engineering

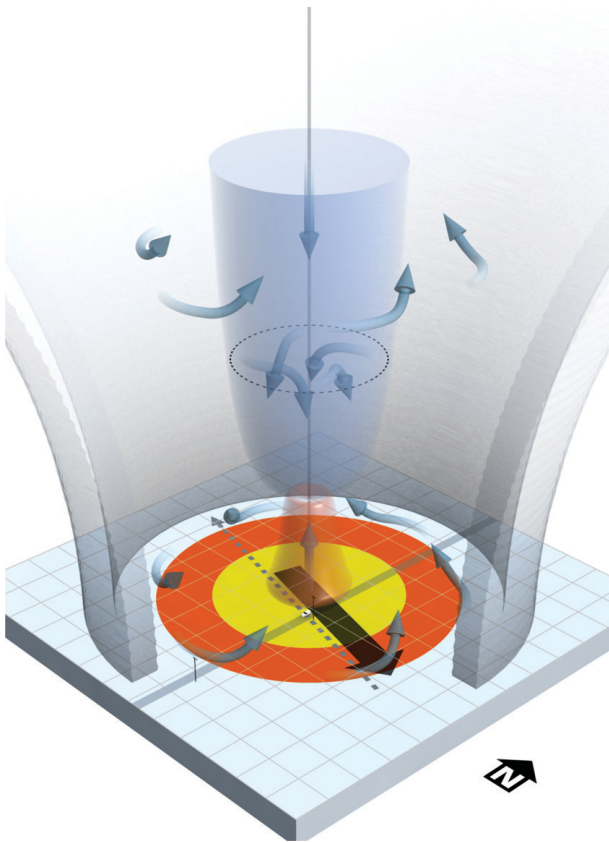


FIG. 9. Three-dimensional structure of the tornado constructed using TIV, DOW, and video data, revealing inward spiraling surface flow and axial downdraft aloft. RMV (orange), RMV_t (yellow), and debris cloud (gray) indicated. Spirally inflowing air slowly rises (red isosurface) near the surface, and is met by an axial downdraft (blue isosurface) below 100 m AGL. TIV, poles along road, and tornado motion/transect indicated.

Center 2006) states very generally that there are “factors . . . which can cause a deviation (either lower or higher) from the expected wind speed for a DOD [degree of damage].” However, in many circumstances it is difficult to determine whether structural failure was concurrent with the occurrence of the maximum wind speeds, or occurred earlier, as in the case of the failure of pole A, or even later. Similarly, it is difficult to distinguish between a failure due to a combination of factors, such as wind and dragging experienced by pole 200S, and a failure due to only locally occurring wind. The video and wind velocity observations in this case show that of the three poles, only pole 100S failed unambiguously due to wind. The current observations document variability in the failure wind speeds for different poles, different damage potential caused by varying wind directions, and/or complex failure modes such as one pole dragging down another, as well as structural failure preceding peak winds.

Additionally, the EF-scale expected value for “broken cross members” is 44 m s^{-1} , and the upper bound is 51 m s^{-1} . These wind speeds were well exceeded at pole A and pole 100S, but neither pole experienced broken cross members prior to pole collapse. Finally, it is important to note that peak DOW radar-observed wind speeds of 72 m s^{-1} , over 20 m s^{-1} stronger than observed by radar during the damage event, occurred about 200 s later near 2214 during a time when the tornado was impacting only open grassland more than 1 km east of the line of poles (Fig. 1), causing no documented damage. More intercomparisons between measured winds and cotemporal damage are needed to evaluate the EF scale’s wind speed values, and the application of the EF scale’s wind–damage relationship to accurately relate structural damage to peak wind gust intensity.

SUMMARY AND CONCLUSIONS. This unique integration of in situ wind measurements, finescale mobile radar measurements, and visual/video evidence has allowed the three-dimensional structure of a tornado, aloft and very near the ground, and the mechanisms by which it caused damage, to be characterized in unique detail. Near-surface convergence to very near the center of rotation, peak tornado and ground-relative winds outside the RMW, and an axial downdraft not penetrating to the surface have been revealed. Observed asymmetries, however, cause deviations from the simple deduced model, and quasiperiodic modulation of intensity is documented. Horizontal wind speeds between the lowest radar-observed levels ($\sim 30 \text{ m AGL}$) and 3.5 m AGL were similar, and therefore it was assumed that these were approximately constant between observation levels.

Complexities in the mechanisms and the time history of damage have illuminated limitations of the operationally employed EF wind–damage scale. Specifically, three nearly identical structures failed at substantially different wind speeds in this tornado, and cross-member damage, predicted at the observed wind speeds, did not occur. One structure failed before peak winds were experienced at that location. Moreover, radar-observed tornado intensity peaked after the occurrence of documented damage, a well-known limitation of damage–intensity-based wind estimation methods. Additional radar and in situ observations in tornadoes in the region $<30 \text{ m AGL}$ (Kosiba and Wurman 2012) will be critical in refining knowledge concerning low-level tornado structure, and the relationship among wind speed, direction, and duration and observed damage.

ACKNOWLEDGMENTS. This analysis was supported by National Science Foundation (NSF) Grants AGS-080401 and -1211132. The Doppler on Wheels Facility is supported by NSF Grant AGS-0734001, and VORTEX2 planning was supported by NSF Grant AGS-724318. The authors thank Sean Casey and the TIV crew for collecting the in situ data, Discovery Channel for the video imagery, and the reviewers, including David Lewellen, for their helpful input. Photograph of TIV by Justin Walker, CSWR. Photograph of DOW with tornado by Herb Stein, CSWR.

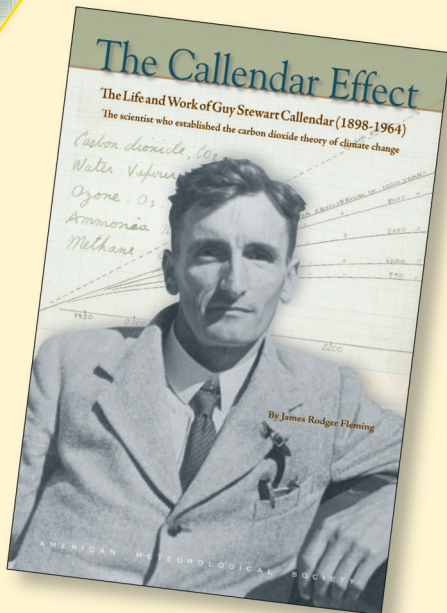
REFERENCES

- Alexander, C. R., and J. Wurman, 2008: Updated mobile radar climatology of supercell tornado structures and dynamics. *Extended Abstracts, 24th Conf. on Severe Local Storms*, Savannah, GA, Amer. Meteor. Soc., 19.4. [Available online at <https://ams.confex.com/ams/pdfpapers/141821.pdf>]
- Atkins, N. A., R. McGee, R. Ducharme, R. M. Wakimoto, and J. Wurman, 2012: The LaGrange tornado during VORTEX 2. Part II: Photogrammetric analysis of the tornado combined with dual-Doppler radar data. *Mon. Wea. Rev.*, **140**, 2939–2958.
- Barnes, S. L., 1964: A technique for maximizing details in numerical weather-map analysis. *J. Appl. Meteor.*, **3**, 396–409.
- Bluestein, H. B., W.-C. Lee, M. Bell, C. C. Weiss, and A. L. Pazmany, 2003: Mobile Doppler radar observations of a tornado in a supercell near Bassett, Nebraska, on 5 June 1999. Part II: Tornado-vortex structure. *Mon. Wea. Rev.*, **131**, 2968–2984.
- , C. C. Weiss, and A. L. Pazmany, 2004: The vertical structure of a tornado near Happy, Texas, on 5 May 2002: High-resolution, W-band, Doppler radar observations. *Mon. Wea. Rev.*, **132**, 2325–2337.
- , —, M. M. French, E. M. Holthaus, R. L. Tanamachi, S. Frasier, and A. L. Pazmany, 2007: The structure of tornadoes near Attica, Kansas, on 12 May 2004: High-resolution, mobile, Doppler radar observations. *Mon. Wea. Rev.*, **135**, 475–506.
- Burgers, J. M., 1948: A mathematical model illustrating the theory of turbulence. *Adv. Appl. Mech.*, **1**, 171–199.
- Church, C. R., and J. T. Snow, 1993: Laboratory models of tornadoes. *The Tornado: Its Structure, Dynamics, Prediction, and Hazards, Geophys. Monogr.*, Vol. 79, Amer. Geophys. Union, 277–295.
- , —, G. L. Baker, and E. M. Agee, 1979: Characteristics of tornado-like vortices as a function of swirl ratio: A laboratory investigation. *J. Atmos. Sci.*, **36**, 1755–1776.
- Davies-Jones, R. P., 1986: Tornado dynamics. *Thunderstorm Morphology and Dynamics*, Vol. 2, *Thunderstorms—A Social, Scientific, and Technological Documentary*, 2nd ed., E. Kessler, Ed., University of Oklahoma Press, 197–236.
- Doswell, C. A., III, H. E. Brooks, and N. Dotzek, 2009: On the implementation of the enhanced Fujita scale in the USA. *Atmos. Res.*, **93**, 554–563.
- Dowell, D. C., C. R. Alexander, J. M. Wurman, and L. J. Wicker, 2005: Centrifuging of hydrometeors and debris in tornadoes: Radar-reflectivity patterns and wind-measurement errors. *Mon. Wea. Rev.*, **123**, 1501–1524.
- Edwards, R., J. G. LaDue, J. T. Ferree, K. Scharfenberg, C. Maier, and W. L. Coulbourne, 2013: Tornado intensity estimation: Past, present, and future. *Bull. Amer. Meteor. Soc.*, in press.
- FEMA, 2012: Mitigation Assessment Team Report—Spring 2011 tornadoes: April 25–28 and May 22—Building performance observations, recommendations, and technical guidance. FEMA P-908, 512 pp. [Available online at www.fema.gov/library/viewRecord.do?fromSearch=fromsearch&id=5633]
- Fiedler, B. H., and R. Rotunno, 1986: A theory for the maximum windspeeds in tornado-like vortices. *J. Atmos. Sci.*, **43**, 2328–2340.
- Fouts, J. L., D. L. James, and C. W. Letchford, 2003: Pressure distribution on a cubical model in tornado-like flow. *Preprints, 11th Int. Conf. on Wind Engineering*, Lubbock, TX, ICWE.
- Haan, F. L., Jr., V. K. Balaramudu, and P. P. Sarkar, 2010: Tornado-induced wind loads on a low-rise building. *J. Struct. Eng.*, **136**, 106–116.
- Howells, P. A. C., R. Rotunno, and R. K. Smith, 1988: A comparative study of atmospheric and laboratory-analogue numerical tornado-vortex models. *Quart. J. Roy. Meteor. Soc.*, **114**, 801–822.
- Kosiba, K. A., and J. Wurman, 2010: The three-dimensional axisymmetric wind field structure of the Spencer, South Dakota, 1998, tornado. *J. Atmos. Sci.*, **67**, 3074–3083.
- , and —, 2012: Near-ground radar and anemometer measurements in the Russell, Kansas (2005) tornado. *Preprints, 26th Conf. on Severe Local Storms*, Nashville, TN, Amer. Meteor. Soc., 16.4. [Available online at <https://ams.confex.com/ams/26SLS/webprogram/Paper211752.html>]
- , R. J. Trapp, and J. Wurman, 2008: An analysis of the axisymmetric three-dimensional low level wind field in a tornado using mobile radar observations. *Geophys. Res. Lett.*, **35**, L05805, doi:10.1029/2007GL031851.

- , J. Wurman, P. Markowski, Y. Richardson, P. Robinson, and J. Marquis, 2013: Genesis of the Goshen County, Wyoming, tornado on 5 June 2009 during VORTEX2. *Mon. Wea. Rev.*, **141**, 1157–1181.
- Kuai, L., F. L. Haan Jr., W. Gallus Jr., and P. P. Sarkar, 2008: CFD simulations of the flow field of a laboratory-simulated tornado for parameter sensitivity studies and comparison with field measurements. *Wind Struct.*, **11**, 75–96.
- Lee, W.-C., and J. Wurman, 2005: The diagnosed structure of the Mulhall tornado. *J. Atmos. Sci.*, **62**, 2373–2393.
- , B. J.-D. Jou, P.-L. Chang, and S.-M. Deng, 1999: Tropical cyclone kinematic structure retrieved from single-Doppler radar observations. Part I: Interpretation of Doppler velocity patterns and the GBVTD technique. *Mon. Wea. Rev.*, **127**, 2419–2439.
- Lewellen, D. C., and W. S. Lewellen, 2007a: Near-surface intensification of tornado vortices. *J. Atmos. Sci.*, **64**, 2176–2194.
- , and —, 2007b: Near-surface vortex intensification through corner flow collapse. *J. Atmos. Sci.*, **64**, 2195–2209.
- , —, and J. Xia, 2000: The influence of a local swirl ratio on tornado intensification near the surface. *J. Atmos. Sci.*, **57**, 527–544.
- , B. Gong, and W. S. Lewellen, 2008: Effects of finescale debris on near-surface tornado dynamics. *J. Atmos. Sci.*, **65**, 3247–3262.
- Lewellen, W. S., 1976: Assessment of knowledge and implications for man. *Proc. Symp. on Tornadoes*, Lubbock, TX, Texas Tech University, 107–143.
- , D. C. Lewellen, and R. I. Sykes, 1997: Large-eddy simulation of a tornado's interaction with the surface. *J. Atmos. Sci.*, **54**, 581–605.
- Lott, N., A. Smith, J. Crouch, T. Houston, and K. Shein, cited 2012: Billion dollar U.S. weather/climate disasters, 1980–2011. Fact sheet, NOAA/National Climatic Data Center. [Available online at www.ncdc.noaa.gov/oa/reports/billionz.html.]
- Markowski, P., and Coauthors, 2012a: The pretornadic phase of the Goshen County, Wyoming, supercell of 5 June 2009 intercepted by VORTEX2. Part I: Evolution of kinematic and surface thermodynamic fields. *Mon. Wea. Rev.*, **140**, 2887–2915.
- , and Coauthors, 2012b: The pretornadic phase of the Goshen County, Wyoming, supercell of 5 June 2009 intercepted by VORTEX2. Part II: Intensification of low-level rotation. *Mon. Wea. Rev.*, **140**, 2916–2938.
- Marquis, J. N., Y. P. Richardson, and J. M. Wurman, 2007: Kinematic observations of mesocyclones along boundaries during IHOP. *Mon. Wea. Rev.*, **135**, 1749–1768.
- McDonald, J. R., G. S. Forbes, and T. P. Marshall, 2004: The enhanced Fujita (EF) scale. Preprints, *22nd Conf. on Severe Local Storms*, Hyannis, MA, Amer. Meteor. Soc., 7.
- Nolan, D. S., and M. T. Montgomery, 2002: Nonhydrostatic, three-dimensional perturbations to balanced, hurricane-like vortices. Part I: Linearized formulation, stability, and evolution. *J. Atmos. Sci.*, **59**, 2989–3020.
- Potter, S., 2007: Fine-tuning Fujita. *Weatherwise*, **60**, 64–71.
- Rott, N., 1958: On the viscous core of a line vortex. *Z. Angew Math. Mech.*, **9**, 543–553.
- Rotunno, R., 1979: A study in tornado-like vortex dynamics. *J. Atmos. Sci.*, **36**, 140–155.
- Selvam, R. P., and P. C. Millett, 2003: Computer modeling of tornado forces on buildings. *Wind Struct.*, **6**, 209–220.
- Simiu, E., and R. H. Scanlan, 1996: *Wind Effects on Structures: Fundamentals and Applications to Design*. John Wiley and Sons, 688 pp.
- Snow, J. T., 1982: A review of recent advances in tornado vortex dynamics. *Rev. Geophys. Space Phys.*, **20**, 953–964.
- Tanamachi, R. L., H. B. Bluestein, W.-C. Lee, M. Bell, and A. Pazmany, 2007: Ground-based velocity display (GBVTD) analysis of W-band Doppler radar data in a tornado near Stockton, Kansas, on 15 May 1999. *Mon. Wea. Rev.*, **135**, 783–800.
- Wakimoto, R. M., N. T. Atkins, and J. Wurman, 2011: The LaGrange tornado during VORTEX2. Part I: Photogrammetric analysis of the tornado combined with single-Doppler radar data. *Mon. Wea. Rev.*, **139**, 2233–2258.
- , P. Stauffer, W.-C. Lee, N. T. Atkins, and J. Wurman, 2012: Finescale structure of the LaGrange, Wyoming, tornado during VORTEX2: GBVTD and photogrammetric analyses. *Mon. Wea. Rev.*, **140**, 3397–3418.
- Wind Science and Engineering Center, 2006: A recommendation for an Enhanced Fujita Scale (EF-Scale). Wind Science and Engineering Center, Texas Tech University, 111 pp. [Available online at www.depts.ttu.edu/weweb/Pubs/fscale/EFScale.pdf.]
- Wurman, J., 2001: The DOW mobile multiple Doppler network. Preprints, *30th Int. Conf. on Radar Meteorology*, Munich, Germany, Amer. Meteor. Soc., 95–97.
- , 2002: The multiple-vortex structure of a tornado. *Wea. Forecasting*, **17**, 473–505.
- , and J. Winslow, 1998: Intense sub-kilometer-scale boundary layer rolls in Hurricane Fran. *Science*, **280**, 555–557.
- , and S. Gill, 2000: Finescale radar observations of the Dimmitt, Texas (2 June 1995), tornado. *Mon. Wea. Rev.*, **128**, 2135–2164.

NEW FROM AMS BOOKS!

WHERE METEOROLOGY MEETS HISTORY!



The Callendar Effect: The Life and Work of Guy Stewart Callendar (1898–1964)

BY JAMES RODGER FLEMING

This is the untold story of the remarkable scientist who established the carbon dioxide theory of climate change. G. S. Callendar discovered that global warming could be brought about by increases in the concentration of atmospheric carbon dioxide due to human activities, primarily through burning fossil fuels. He did this in 1938! Using never-before-published original scientific correspondence, notebooks, family letters, and photographs, noted science historian James Rodger Fleming gives us the life and work of this leading British engineer, through the World Wars and beyond, to Callendar's continuing legacy as the scientist who established the Callendar Effect.

LIST \$34.95 MEMBER \$24.95 © 2007, HARDCOVER, 176 PGS, HM, AMS CODE: CLDR
ISBN 10: 1-878220-76-4, ISBN 13: 978-1-878220-76-9

ALSO ON DVD! The Papers of Guy Stewart Callendar

EDITED BY JAMES RODGER FLEMING AND JASON THOMAS FLEMING

This research-quality digital archive of Guy Stewart Callendar's manuscript letters, papers, journals, documents, and family photographs—including extensive weather and climate data—is an essential tool for historians, climate scientists, and other scholars, and a desirable acquisition for libraries.

PRICE AVAILABLE UPON REQUEST, AMS CODE: CLDR DVD
© 2007, DVD, ISBN 10: 1-878220-80-2, ISBN 13: 978-1-878220-80-6

ORDER TODAY!

www.ametsoc.org/bookstore

Or see the order form at the back of this magazine.

AMS BOOKS
RESEARCH APPLICATIONS HISTORY

- , and T. Samaras, 2004: Comparison of in situ pressure and DOW Doppler winds in a tornado and RHI vertical slices through 4 tornadoes during 1996–2004. *Extended Abstracts, 22nd Conf. on Severe Local Storms*, Hyannis, MA, Amer. Meteor. Soc., 15.4. [Available online at https://ams.confex.com/ams/11aram22sls/techprogram/paper_82352.htm.]
- , and C. Alexander, 2005: The 30 May 1998 Spencer, South Dakota storm. Part II: Comparison of observed damage and radar-derived winds in the supercell tornadoes. *Mon. Wea. Rev.*, **133**, 97–119.
- , and K. A. Kosiba, 2008: DOW observations of multiple vortex structure in several tornadoes. *Extended Abstracts, 24th Conf. on Severe Local Storms*, Savannah, GA, Amer. Meteor. Soc., P3.20. [Available online at <https://ams.confex.com/ams/pdfpapers/142194.pdf>.]
- , J. Straka, and E. Rasmussen, 1996: Fine-scale Doppler radar observation of tornadoes. *Science*, **272**, 1774–1777.
- , —, —, M. Randall, and A. Zahrai, 1997: Design and deployment of a portable, pencil-beam, pulsed, 3-cm Doppler radar. *J. Atmos. Oceanic Technol.*, **14**, 1502–1512.
- , C. Alexander, P. Robinson, and Y. Richardson, 2007a: Low-level winds in tornadoes and potential catastrophic tornado impacts in urban areas. *Bull. Amer. Meteor. Soc.*, **88**, 31–46.
- , Y. Richardson, C. Alexander, S. Weygandt, and P. F. Zhang, 2007b: Dual-Doppler and single-Doppler analysis of a tornadic storm undergoing mergers and repeated tornadogenesis. *Mon. Wea. Rev.*, **135**, 736–758.
- , —, —, —, and —, 2007c: Dual-Doppler analysis of winds and vorticity budget terms near a tornado. *Mon. Wea. Rev.*, **135**, 2392–2405.
- , P. Robinson, W. Lee, C. R. Alexander, and K. A. Kosiba, 2008: Rapid-scan mobile radar 3D GBVTD and traditional analysis of tornadogenesis. *Extended Abstracts, 24th Conf. on Severe Local Storms*, Savannah, GA, Amer. Meteor. Soc., P13.6. [Available online at https://ams.confex.com/ams/24SLS/techprogram/paper_142176.htm.]
- , K. A. Kosiba, P. Markowski, Y. Richardson, D. Dowell, and P. Robinson, 2010: Finescale and dual-Doppler analysis of tornado intensification, maintenance, and dissipation in the Orleans, Nebraska, supercell. *Mon. Wea. Rev.*, **138**, 4439–4455.
- , D. Dowell, Y. Richardson, P. Markowski, E. Rasmussen, D. Burgess, L. Wicker, and H. B. Bluestein, 2012: The Second Verification of the Origins of Rotation in Tornadoes Experiment: VORTEX2. *Bull. Amer. Meteor. Soc.*, **93**, 1147–1170.